archives
of thermodynamics
Vol. **44**(2023), No. 4, 197–220
DOI: 10.24425/ather.2023.149715

Numerical investigations of transient thermal loading of steam turbines for SMR plants

MARIUSZ BANASZKIEWICZ*
MICHAŁ SKWARŁO

Institute of Fluid Flow Machinery, Polish Academy of Sciences,
Fiszera 14, 80-231 Gdańsk, Poland

Abstract One of the well-known technologies that fit well into the goal of reduction of greenhouse gas emissions is nuclear energy. In particular, the change in approach to the design and construction of nuclear power plants led to the development of small modular reactors (SMRs), which are characterized by a broader range of possible applications than large nuclear reactors and the ability to flexibly operate as per load demand. This paper presents an analysis of the thermal loads of a steam turbine rotor operating in a power plant with SMR. Steam-water cycle and turbine train of a 300 MW unit are presented. High-pressure steam turbine rotor and its thermal loading due to varying steam conditions are investigated for a cold start-up designed with consideration of the thermal characteristics of nuclear reactors. It was shown by numerical simulations that steam condensation on rotor surfaces plays a crucial role in determining its thermal behaviour. Comparison with conventional rotors has shown that the thermal loading of nuclear turbine rotors is lower and more stable than that of conventional turbines.

Keywords: Nuclear turbine; Small modular reactor; Heat transfer; Steam condensation

Nomenclature

Bi	–	Biot number
c_p	–	specific heat, J/(kg K)
d	–	characteristic diameter, m

*Corresponding Author. Email: mbanaszkiewicz@imp.gda.pl

g	–	heat source, W/m^3
h	–	specific enthalpy, J/kg
k	–	thermal conductivity, W/(m K)
Nu	–	Nusselt number
p	–	pressure, Pa
Pr	–	Prandtl number
r	–	radial coordinate, m
Re	–	Reynolds number
s	–	specific entropy, J/(kg K)
T	–	temperature, K
t	–	time, s
z	–	axial coordinate, m

Greek symbols

α	–	heat transfer coefficient, W/(m^{2}K)
ρ	–	density, kg/m^3
ω	–	rotational velocity, rpm

Subscripts

cond	–	condensation
conv	–	convection
f	–	fluid
s	–	surface
sat	–	saturation
st	–	steam

Abbreviations

BWR	–	boiling water reactor
GHG	–	greenhouse gases
HP	–	high pressure
IAEA	–	International Atomic Energy Agency
LP	–	low pressure
LWGR	–	light water-cooled graphite moderated reactor
PHWR	–	pressurized heavy water reactor
PWR	–	pressurized water reactor
SMR	–	small modular reactor
STG	–	steam turbine and generator

1 Introduction

The power sector, similarly to other branches of industry, has a different structure in different countries. However, in the global view, it is common for most countries that the power sector is one of the largest contributors

of harmful wastes and greenhouse gas (GHG) emissions to nature [1]. According to the International Atomic Energy Agency (IAEA) projection it is expected that electricity demands will double by 2050 [2]. This forecast makes governments, industrial companies, and people around the world even more aware of the need for an energy transformation whose main goal is to achieve net-zero GHG emissions.

The key point is an optimal energy mix (various in different countries), in which the power sector is co-created by renewable energy sources and traditional power plants. One type of traditional power plant is a nuclear plant. The nuclear power units are based on a well-known design and proven technology. They are used to generate electricity as well as for district heating purposes in cogeneration systems [3,4]. The main advantages of nuclear power are as follows: a reliable and secure power that in many countries is fully competitive, moreover, a technology that in normal operation is environmentally benign with zero carbon emissions (the electricity generation process is free of combustion) [5,6]. In comparison to the other conventional power units, nuclear energy has an advantageous position for two main reasons: a longer lifetime of nuclear resources and very small GHG emissions for the nuclear chain (whole cycle of resources management) [7,8].

According to the IAEA, more than 400 nuclear power plants are in service (in thirty countries) and generate approximately 10% of global electricity (data until 2022) [2]. The vast majority of these units are large power plants and over 90% of them are equipped with light water pressurized reactors and boiling water reactors (PWR and BWR, respectively) [5,9]. Nevertheless, regardless of reactor technology, large nuclear units are characterized by a long time of the design and construction phase, a high share of work needed to be performed on-site, and large capital investment. All these factors make this type of power plant lose its attractiveness, in particular to private companies and investors.

The mentioned disadvantages of large nuclear power plants could be eliminated by small modular reactors (SMR). SMRs are defined as advanced nuclear reactors that have a power capacity of up to 300 MW(e) per unit [10]. However, there are also SMRs with greater power output – up to $\sim$ 500 MW(e). SMRs, which can produce a large amount of low-carbon electricity are: i) small (physically a fraction of the size of a conventional nuclear power reactor), ii) modular (making it possible for systems and components to be factory-assembled and transported as a unit to a location for installation), iii) reactors (harnessing nuclear fission to generate heat to produce energy) [10]. In addition to reduced time of design and con-

struction phase [11], usage of prefabricated modules, and saving on cost, the advantage of SMRs is also a wider field of possible applications. Similarly to large nuclear units, the SMRs can be used for electricity generation and district heat (cogeneration systems), but also for various industrial applications (due to their modularity and ability to flexible operation as per load demand).

The nuclear reactors, and especially SMRs, are also considered in the context of a process known as 'retrofit decarbonization' of existing coal power plants. This term, retrofit decarbonization, includes the use of carbon capture, fuel conversion, and the replacement of coal boilers with new low-carbon energy sources [9]. One of the main goals is also re-using the existing equipment of coal power plants to the extent that is economically justified [12]. This process is of particular importance for the Polish energy sector due to the extensive fleet of coal units. The possibility of using SMRs for retrofit decarbonization has been described and analyzed in several recently published papers. The common conclusion of these works is that the high-temperature reactors (which constitute a significant part of the SMRs being developed [13]) seem to be suited best for this purpose because of their ability to provide high parameters of steam [9, 14]. Application of SMRs based on light water reactor technology for repowering a coal power plant is also possible, but due to lower steam parameters it is more difficult (extensive modernization of steam turbine unit is required) and less economically attractive [11].

In terms of power capacity, the idea of small or medium-sized reactors is nothing new. Table 1 shows some examples of small reactors for different steam turbine and generator (STG) power outputs, that are in operation [15]. The table includes pressurized water reactors (PWRs), light water-cooled graphite moderated reactor (LWGR) and pressurized heavy water reactor (PHWR).

Table 1: Small nuclear reactors in operation.

Name	STG power output	Type	Country
EGP-6	11 MW(e)	LWGR	Russia
KLT-40S	35 MW(e)	PWR	Russia
RITM-200	50 MW(e)	Integral PWR	Russia
PHWR-220	220 MW(e)	PHWR	India
CNP-300	300 MW(e)	PWR	China, Pakistan

These types of reactors are based on the same technologies as large reactors (mainly PWR and BWR). In the case of SMRs, the change primarily concerns the approach to the design and construction phases (modular design) in order to save time and cost. As the SMR units are currently mostly in the design and development phase, there is also a change in the use of different reactor technologies. The IAEA advance reactor database [13] provides a list of approximately eighty SMRs (some of them already under construction). The list includes examples of well-known light water reactors, as well as new-generation reactors (high-temperature reactors).

Table 2 presents some examples of SMRs developed using conventional nuclear fuel and cooling technology (PWR and BWR reactors) with a high probability of deployment in the first half of the next decade [1, 15].

Table 2: Small modular reactors in an advanced stage of development.

Name	STG power output	Type	Developer, country
NuScale Power Module	77 MW(e)	Integral PWR	NuScale, USA
Nuward	180 MW(e)	PWR	EDF + TechnicAtome, France
SMR-160	160 MW(e)	PWR	Holtec, USA + SNC-Lavalin, Canada
BWRX-300	300 MW(e)	BWR	GE Hitachi, USA
Candu SMR	300 MW(e)	PHWR	SNC-Lavalin, Canada
Rolls-Royce SMR	500 MW(e)	PWR	Rolls-Royce, UK

In terms of steam parameters (pressure, temperature) at the steam generator outlet, they do not differ from parameters achieved in large units [16,17]. However, the main difference is noticeable regarding the steam mass flow rate. A comparison of a few large PWR and BWR reactors with SMR reactor BWRX-300 is presented in Table 3.

Lower mass flow of steam also results in lower volumetric flow at low-pressure (LP) turbine exhaust. Additionally, considering the main design assumptions of SMR – modular and compact components as far as possible factory assembled, steam turbine for SMR units will be full speed machine with 3000 rpm or 3600 rpm operation speed. This is a significant difference compared to half-speed steam turbines in large nuclear units, which causes operation in wet steam conditions to become even more of a challenge and needs additional attention in the case of SMR units based on PWR or BWR technology [22].

Table 3: Steam parameters at steam generator outlet in large nuclear reactors and SMR.

		Power plant with nuclear reactor				
		APR-1400 [18]	EPR-1600 [18]	ABWR [19]	ESBWR [20]	BWRX-300 [21]
	Reactor type	PWR	PWR	BWR	BWR	SMR BWR
Steam generator outlet:	Pressure (MPa)	6.84	7.80	7.07	7.17	7.20
	Temperature (°C)	284.3	293.0	287.8	287.7	288.0
	Mass flow rate (kg/s)	2261	2443	2122	2432	470

Calculations for nuclear power plants are carried out mainly for the design point. It is very difficult to find papers concerning off-design conditions of nuclear power plants, except papers discussing the effect of cooling water temperature on the performance of a nuclear power plant [23, 24]. This problem concerns both large nuclear units and SMR units, but it is particularly important concerning the latter due to the wider range of possible applications and greater requirements for operational flexibility.

The main objective of this paper is to investigate the thermal loads of a high-pressure steam turbine rotor operating in an SMR power plant with a BWR reactor. The choice of this type of nuclear reactor is driven by the fact that, currently, the SMR developed by GE Hitachi Nuclear Energy, BWRX-300, seems to be one of the closest to being implemented into the Polish energy system in the near future [25]. Calculations concerning off-design conditions and, especially, transient conditions are crucial in terms of fatigue assessment of steam turbine components [26]. Calculations presented in this paper include analysis of thermal loads of the HP rotor during operation at transient conditions – steam turbine start-up. Understanding the thermal behaviour of such rotors is critical for determining the operational flexibility of SMR units, which is one of the most demanded features for future applications.

2 Steam turbine for SMR unit

2.1 Thermal cycle and steam turbine modules

This paper presents the results of analyses carried out for a steam turbine operating in a steam-water cycle with SMR based on BWR technology. This kind of cycle contains the same main components as a cycle with a large

BWR, including a nuclear reactor (steam generator), steam turbine and generator, moisture separator and reheater, condenser, feedwater heaters and pump [16, 17]. A simplified steam-water cycle with SMR BWRX-300 is presented in Fig. 1. In addition, exemplary steam/water parameters are shown in the diagram.

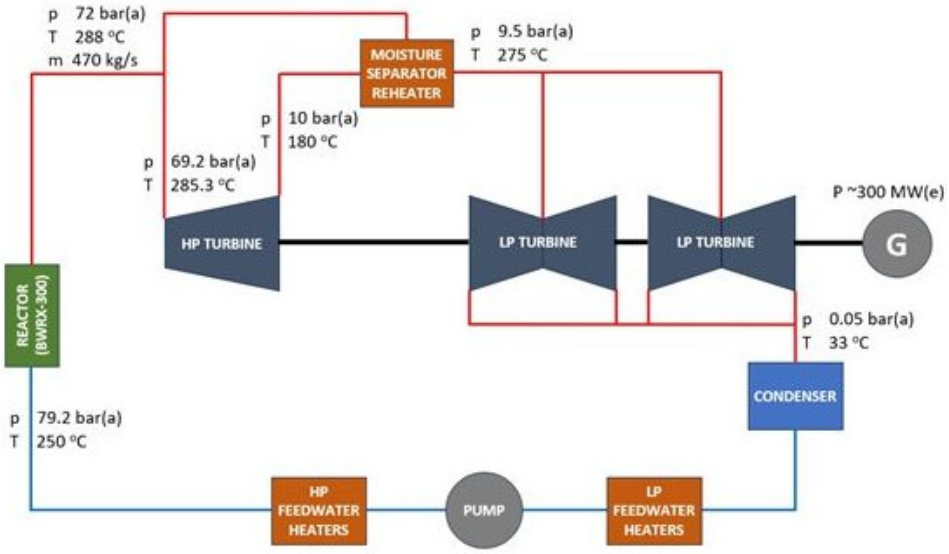

Figure 1: Simplified steam-water cycle with SMR based on BWR technology.

As stated in the definition of SMR, the power capacity of one unit is up to 300 MW(e) (although units with higher power output are also planned). Depending on steam parameters and nominal power output, the steam turbine for the SMR unit may have different configurations. It could be a single casing turbine (combined high pressure (HP) and low pressure (LP) parts) or a multi-casing machine (HP module and one or more LP modules). Possible configurations of a steam turbine for SMR unit based on PWR/BWR technology are presented in Fig. 2.

Referring to Table 3, in BWR/PWR SMR units the steam turbine (HP module) will receive saturated steam at the inlet. This situation occurs for the nominal operating conditions, as well as for partial loads. In these conditions, when analyzing the thermal loads of the HP turbine rotor, a condensation phenomenon (condensation heat transfer model) should be taken into account.

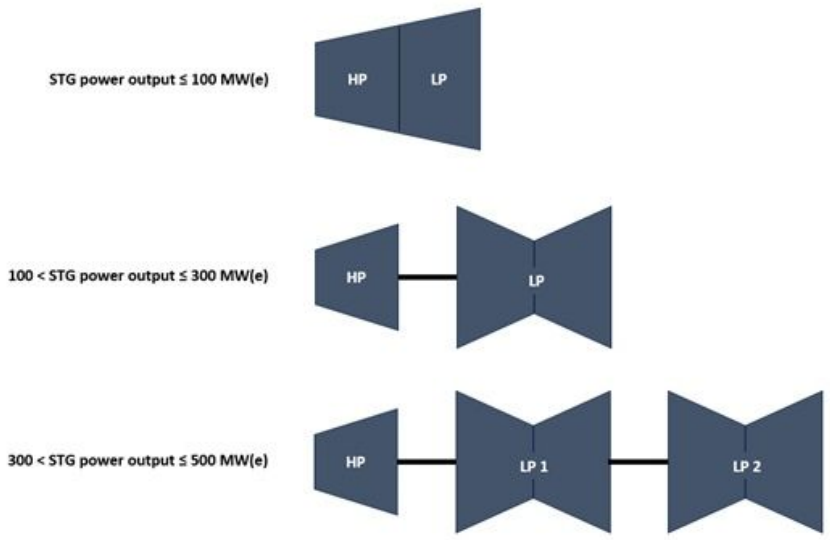

Figure 2: Possible configurations of steam turbine for SMR PWR/BWR power plant.

2.2 High-pressure turbine rotor

For the analyzed 300 MW SMR unit, a turbine train with one HP module and two double flow LP modules is adopted. The HP module is single flow and has drum-type rotor with reaction blading as shown in Fig. 3. In the proposed design, the rotor has 10 stages with reaction blades fixed to the rotor by means of a T-root. Two-stage balance piston (high and low) is

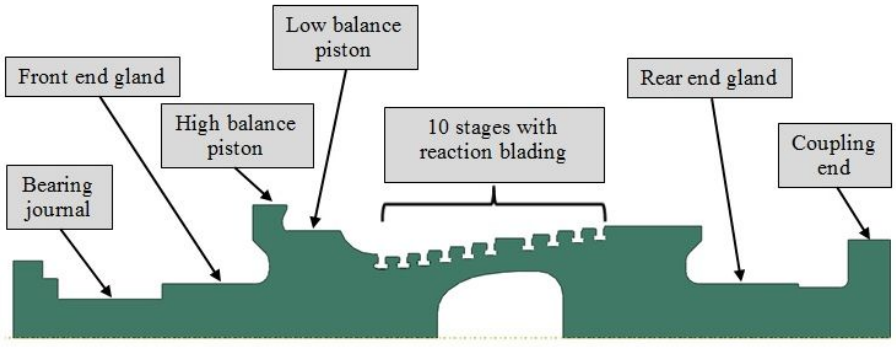

Figure 3: High-pressure turbine rotor.

designed to compensate the axial force generated by pressure drop across the blading. End glands (front and rear) are located on both sides of the rotor. The bearing journal is located at the left end of the rotor while the right end has a coupling end connecting the rotor with the LP module.

Performed calculations indicate that during a transient event – cold start-up of the steam turbine, there is saturated steam at the turbine inlet for most of the time of the turbine loading phase. Only at the beginning of this phase (at very low load, less than 15% of nominal load) the steam at the turbine inlet is slightly superheated. Expansion lines for nominal conditions and transient events (beginning of turbine start-up) are presented in Fig. 4.

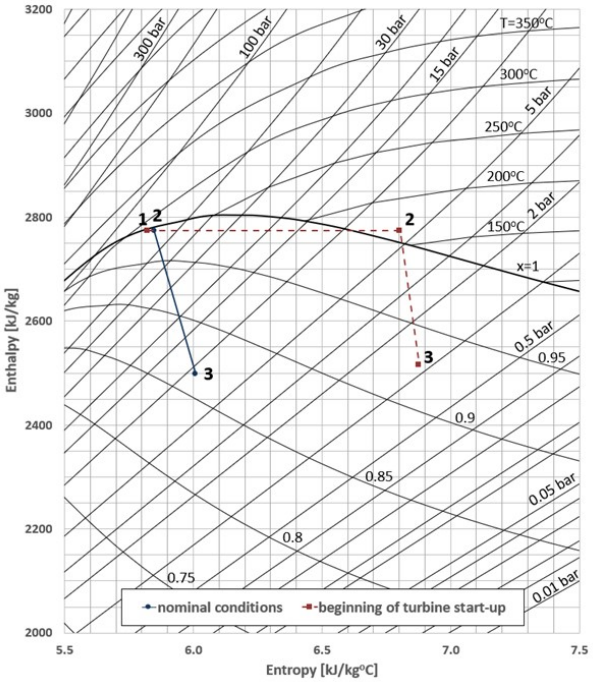

Figure 4: Enthalpy-entropy ($h - s$) diagram, expansion lines for nominal and transient conditions (beginning of turbine start-up) of SMR BWR unit: 1-2 – pressure drop at HP turbine valves, 2-3 – expansion line of HP turbine.

Steam temperatures in the HP turbine at different load conditions are presented in Fig. 5. As stated in the preceding section, the live steam is at the saturation line and its thermodynamic state is maintained during the whole start-up. Steam throttling in the control valves results in little steam

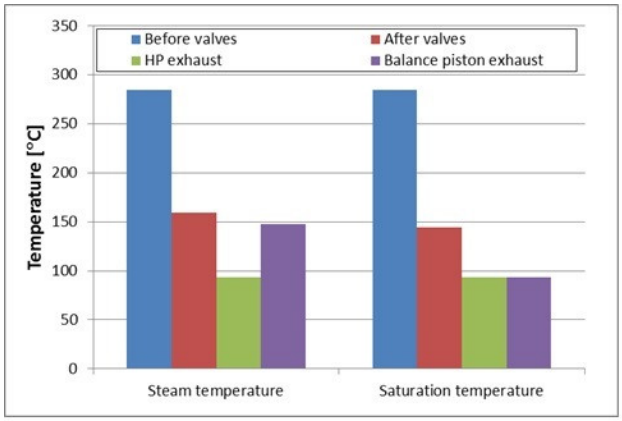

(a)

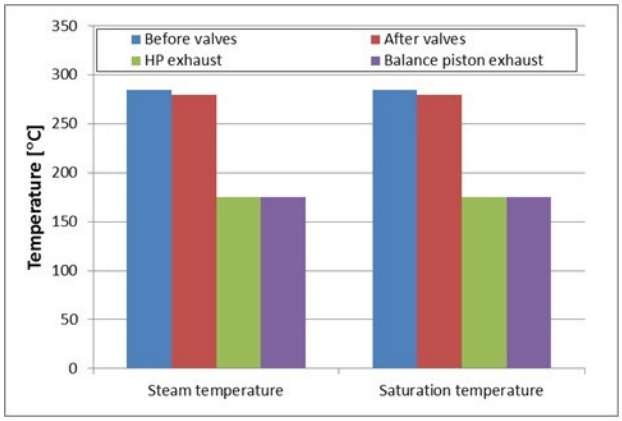

(b)

Figure 5: Steam temperature and saturation temperature in HP turbine at (a) 3000 rpm and no load, (b) 3000 rpm and 300 MW.

superheating at the turbine inlet at the beginning of start-up which diminishes with time and saturated steam conditions are reached at a certain load. Even larger superheating exceeding 50°C occurs at the exhaust of the rotor balance piston and also decreases during loading-up but is still around 1°C at full load. Steam superheating decreases with time along the steam path and at the HP turbine exhaust the saturated steam conditions are present during the whole start-up (similar to the live steam condition). This varying thermodynamic state of steam in the HP turbine is taken into account in further thermal analyses and shown to have a significant impact

on the thermal load of the HP rotor under consideration. In particular, steam condensation on rotor surfaces plays a crucial role in determining its thermal behaviour.

In the case of conventional turbines, steam superheating during start-up and loading increases, and condensation may occur at an early phase of start-up. It is thus an inverse situation as compared to nuclear turbines.

3 Problem formulation

The problem under consideration is the transient heating-up of a nuclear steam turbine rotor taking place during start-up and loading. Rotor heating is caused by steam flow through the turbine with varying temperature, pressure and velocity. Non-stationary heat transfer takes place via forced convection and the thermal load is the primary load of the rotor. The rotor rotates with a constant rotational speed ω in steady-state operation.

The rotor material is assumed isotropic and its physical properties are temperature dependent. The heating process is described by the linear theory of heat conduction and non-linear convective boundary conditions. Due to the geometrical and loading symmetry of the rotor about its axis, the computational region is assumed axisymmetric.

Based on the above assumptions a boundary problem of heat conduction is formulated [27, 28] and solved using a finite element method [29].

3.1 Heat conduction problem

Heat conduction in a homogeneous isotropic solid is described by the Fourier-Kirchhoff differential equation [30]:

$$\operatorname{div}\left[k\operatorname{grad}T(x,t)\right] + g(x,t) = \rho c_p \frac{\partial T(x,t)}{\partial t}\,, \tag{1}$$

where T is the metal temperature, k is the thermal conductivity, g is the heat source, ρ is the density, and c_p is the specific heat.

Neglecting the heat source g and assuming heat conduction in the radial and axial direction only, Eq. (1) is re-written in a cylindrical coordinate system as follows:

$$\rho c_p \frac{\partial T}{\partial t} = \frac{1}{r}\frac{\partial}{\partial r}\left(kr\frac{\partial T}{\partial r}\right) + \frac{\partial}{\partial z}\left(k\frac{\partial T}{\partial z}\right), \tag{2}$$

where r represents the radial coordinate, and z is the axial direction. A non-uniform temperature distribution $T(r, z)$ is assumed as the initial condition at $t = 0$. For rotor-free surfaces, the boundary conditions are:

$$\left.\frac{\partial T}{\partial r}\right|_{r=0} = 0 \qquad \text{for} \quad t \geq 0, \tag{3}$$

$$k(z,t)\left.\frac{\partial T}{\partial r}\right|_{r=r_{\text{out}}(z)} = -\alpha(z,t)\left(T_s - T_f(z,t)\right) \qquad \text{for} \quad t \geq 0, \tag{4}$$

where $\alpha(z, t)$ is the heat transfer coefficient varying with time and axial coordinate, T_s is the surface temperature, and $T_f(z, t)$ is the fluid temperature depending on time and axial coordinate. The outer radius of the rotor $r(z)$ varies with the axial coordinate z defining its outer contour.

The material physical properties are temperature-dependent and their variation is described by polynomial functions.

The variation of heat transfer coefficient in time and space $\alpha(z, t)$ is considered by the Nusselt number (Nu), changing in time as a function of the Reynolds number (Re) and Prandtl number (Pr):

$$\text{Nu} = f(\text{Re}, \text{Pr}). \tag{5}$$

The Nusselt number is defined as follows:

$$\text{Nu} = \frac{\alpha d}{k}, \tag{6}$$

where d denotes a characteristic diameter. A detailed form of Eq. (6) depends on the surface type and flow character [31]. The heat transfer model adopted in this study is based on the well-proven formula for heat transfer coefficients in steam turbine rotors [32].

The geometrical model of the rotor is shown in Fig. 6.

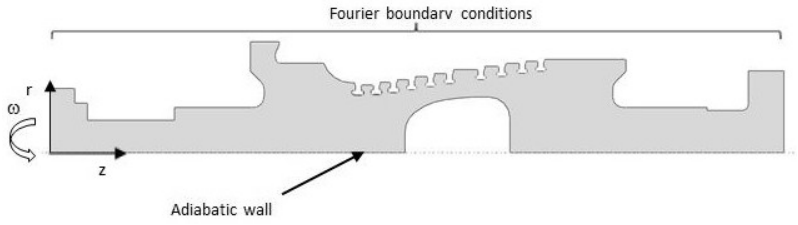

Figure 6: Rotor model with thermal boundary conditions.

3.2 Condensation model

Steam condensation on rotor surfaces can occur when steam is superheated or saturated. In this study, a film condensation mechanism is assumed. A schematic illustration of the condensation model adopted in this work is shown in Fig. 7. If the surface temperature is lower than the saturated steam temperature at the corresponding steam pressure, then steam condenses on the surface. The heat transfer to the surface is intensified as a result of the water film appearing on the surface at the saturated steam temperature, and the heat released due to condensation.

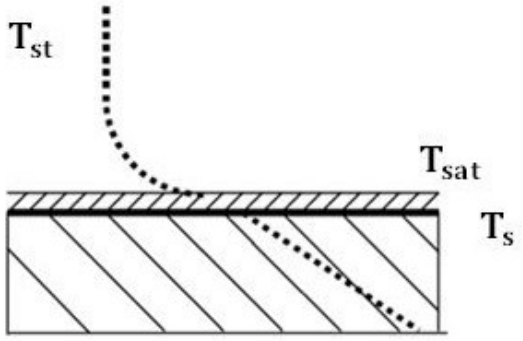

Figure 7: Schematic illustration of film condensation model.

Condensation occurs if the following conditions are satisfied [33–35]:

- the metal surface temperature is below the saturation temperature (T_{sat}) at the local pressure p

$$T_{\mathrm{sat}} > T_s\,, \tag{7}$$

- the heat flux from water film to metal is greater than the heat flux from steam to the water film

$$\alpha_{\mathrm{cond}}\left(T_{\mathrm{sat}} - T_s\right) > \alpha_{\mathrm{conv}}\left(T_{\mathrm{st}} - T_{\mathrm{sat}}\right), \tag{8}$$

where T_{st} denotes steam temperature.

As concluded in [31], available correlations for Nusselt number for simple geometries, like a flat wall or pipe, can be used for estimating condensation heat transfer coefficient usually with a large error. However, it is known that heat transfer coefficients during steam condensation assume large values

reaching 120 000 W/(m^{2}K) in extreme cases during nucleate condensation of steam [36, 37] and, consequently, the errors of their estimation will only slightly affect the variations of temperature and thermal stress fields in turbine components. It was shown that for Biot number Bi $>$ 20, the variation of the heat transfer coefficient has little influence on the variation of temperature distribution [31]. Due to the lack of proper correlations for real turbine geometries (e.g. labyrinth seals, rotating cylinders) and taking into account the above conclusions, the analyses of condensation heat transfer were performed with constant heat transfer coefficient $\alpha = 11\,000$ W/(m^{2}K). This value is within the range of heat transfer coefficients predicted by Shah [38] for film condensation of water inside pipes.

4 Numerical simulations

4.1 Cold start-up parameters

Nuclear steam turbines, similar to conventional turbines, undergo start-ups from various initial thermal conditions. The initial thermal state depends on the cool-down time. The main difference between nuclear and conventional units is in live steam temperature and the resulting metal temperature at the hottest sections of the turbine at the beginning of natural cooling. The live steam temperature for BWR reactors is around 290°C and it determines the hot state of the turbine and initial thermal conditions prior to shut-down. This temperature level corresponds to a typical warm state of conventional turbines which is reached after approximately 30 hours of natural cooling. However, the very cold state of both turbines is defined by the same temperature level with a minimum value of 20°C. This start-up type is assumed in this work for detailed investigations.

Figure 8 presents the proposed cold start-up diagram for a 300 MW steam turbine with the BWRX-300 reactor. This diagram describes variations in time of the rotational speed, power output and live steam temperature and pressure. In large nuclear units, steam turbine start-up is conducted with nominal live steam temperature and pressure, and similar conditions are proposed for the SMR turbines. The rotational speed and power output curves are derived based on the start-up diagrams of 360 MW turbines operating at power plants in Poland [39–41].

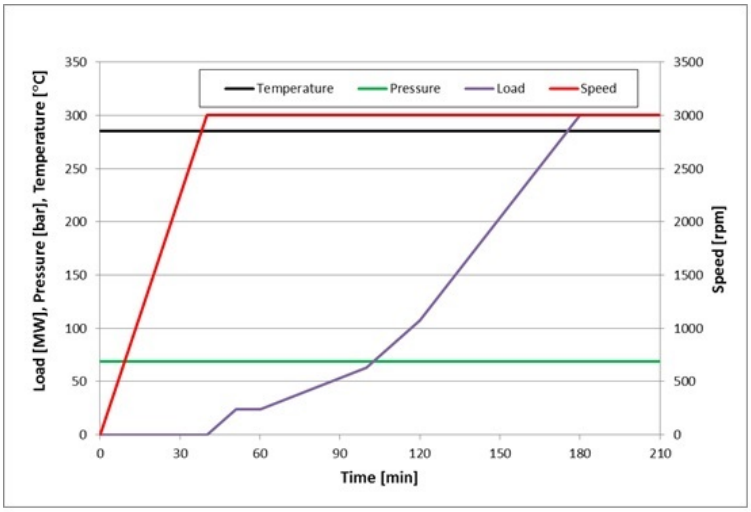

Figure 8: Cold start-up diagram.

4.2 Results and discussion

Numerical calculations have been performed using Abaqus finite element code [42]. Live steam temperature and pressure during start-up were kept constant as shown in Fig. 8, while steam parameters at the rotor inlet were changing during start-up due to steam throttling in the control valves. Temperature distributions in the rotor during start-up from a cold state are shown in Fig. 9. Each plot presents temperature distribution corresponding to one of the characteristic time points of the start-up diagram in Fig. 8. Uniform rotor temperature of 20°C was assumed as an initial condition ($t = 0$ min). After reaching 3000 rpm, the temperature distribution becomes non-uniform and rotor temperature exceeds 100°C at steam inlet sections ($t = 40$ min). For the following 20 minutes ($t = 50$ min and $t = 60$ min), the temperature field remains nearly unchanged as there is little change in steam temperature and mass flow during initial loading. Up to this time, predominantly radial temperature gradients are observed in the rotor body. Further turbine loading, accompanied by steam temperature and mass flow rate increase, brings about a rotor temperature increase up to approximately 200°C at steam inlet sections ($t = 100$ min). Further loading up to 100 MW ($t = 120$ min) does not cause a significant increase in temperature and its distribution in the inlet sections becomes more uniform with diminishing radial temperature gradients. The last 60 minutes of

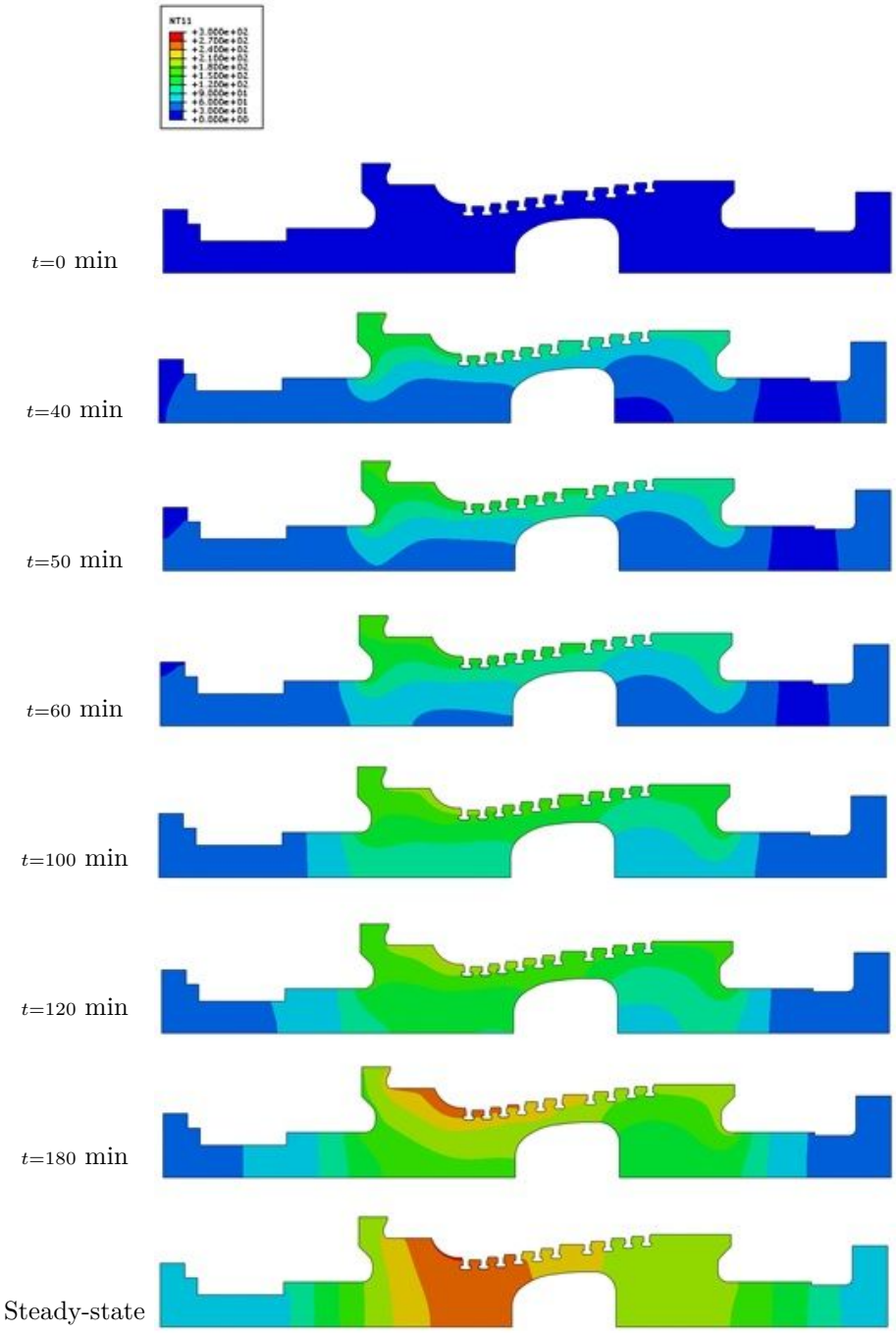

Figure 9: Rotor temperature distributions during cold start-up.

turbine start-up proceeds at an increased loading rate and at reaching nominal load, radial temperature gradients re-occur and rotor inlet surface temperature exceeds 270°C. The temperature distribution is still non-uniform in the steam inlet sections, while the exhaust regions downstream of the cavity are at nearly constant temperature. At time $t = 180$ min, nominal steam mass flow, temperature and pressure upstream of the HP blading are reached and subsequent temperature variations and rotor thermal stabilization take place at constant boundary conditions. At a steady state, a non-uniform temperature field persists in the rotor but radial temperature gradients practically disappear and only axial gradients generated by steam expansion in the HP blading exist.

The presented rotor temperature distributions during turbine start-up show that the highest metal temperatures, their rates of change and gradients occur at the rotor inlet sections, i.e. inlet channel, first blade grooves and balance pistons. These are the most thermally loaded regions of the rotor where the largest heat fluxes from steam to the rotor surfaces are transferred. Consequently, the highest thermal stresses which may lead to fatigue cracking are expected in these regions.

The thermal behaviour of the rotor was investigated in detail for the region of the first rotor gland (between 1st and 2nd blade groove). Steam and metal temperature variations during the cold-start are plotted in Fig. 10. Live steam temperature is kept constant according to the start-up diagram in Fig. 8 and throttling in the control valves at the beginning of run-up results in a steam temperature drop at the turbine inlet (downstream control valves) from nominal value to approximately 150°C. As presented in Section 2, at the early phases of start-up the steam is superheated and its superheating drops with time and vanishes after approximately 50 minutes. Steam condensation occurs immediately after opening the control valves, rotor surface temperature rises above the saturation temperature and further heating takes place due to heat convection from superheated steam to metal. After 40 minutes condensation re-occurs as the steam superheating significantly decreases with a simultaneous decrease of the temperature difference between the rotor surface and saturation temperature. From this time on, rotor surface temperature follows the saturation temperature increasing with steam pressure rise. This is the effect of a large heat transfer coefficient at steam condensation.

The effect of condensation on rotor temperature variations is shown in Fig. 11. The rotor surface temperature from Fig. 10 is plotted together with the mid-wall temperature (at half rotor radius at the first gland) and

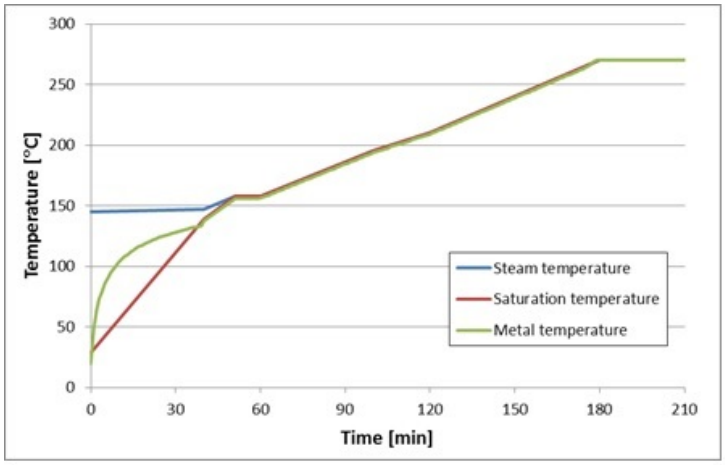

Figure 10: Steam and metal temperature variations at the first rotor gland.

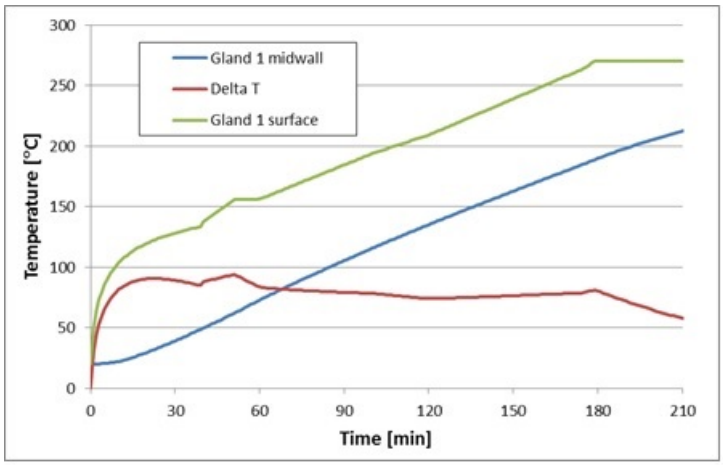

Figure 11: Metal temperature variations at first rotor gland.

their difference. The rotor surface temperature rapidly rises at the beginning of start-up while the mid-wall temperature response is delayed due to rotor thermal inertia and heat resistance. Non-linear transient effects diminish with time and after approximately 20 minutes (10% of start-up time) quasi-steady state conditions prevail. Nearly linear temperature variations are observed and, consequently, the temperature difference remains almost constant. At such conditions, thermal stresses are expected to be

constant and dependent on temperature rate. These conditions prevail simultaneously with steam condensation, and thus the temperature rate linearly depends on the steam pressure rate.

Qualitative and quantitative differences between nuclear and conventional rotor thermal behaviour are observed when considering surface heat fluxes. A comparison of surface heat flux densities in different regions of the nuclear and conventional rotor is presented in Fig. 12. The results for the conventional rotor were obtained assuming a cold start-up diagram for an intermediate pressure turbine with a rotor of similar design which was a basis for designing the high-pressure nuclear rotor investigated in this

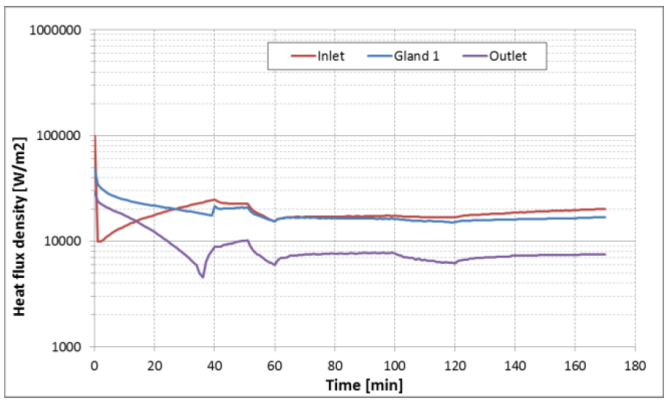

(a)

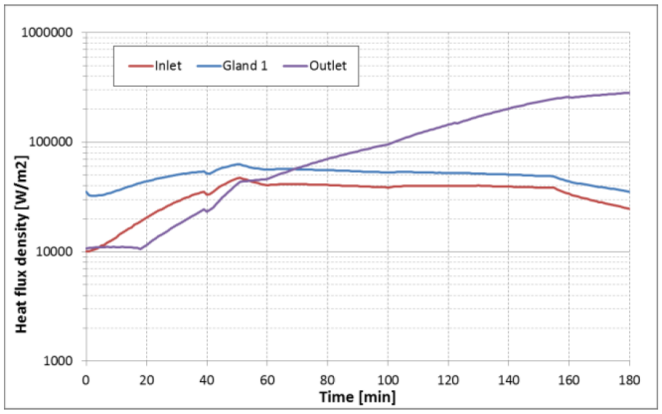

(b)

Figure 12: Variations of surface heat flux densities in rotor different regions (inlet, gland 1 and outlet) for (a) nuclear and (b) conventional steam turbine rotor.

paper. As it is seen from the figures, the heat fluxes in the nuclear rotor initially decrease and after approximately 60 minutes remain constant in the range of 9000–20 000 W/m^2. Only at the beginning of start-up, very high heat flux densities reaching 100 000 W/m^2 are calculated due to the large condensation heat transfer. A different picture is seen for the conventional rotor where the initial values of heat fluxes are relatively low in the range of 9000–20 000 W/m^2 and subsequently increase to approximately 50000 W/m^2 after 60 minutes. They remain almost constant in some regions (gland, inlet) or even increase to 300 000 W/m^2 at the end of start-up. The above analysis proves that the thermal loading of nuclear turbine rotors is lower and more stable than that of conventional rotors.

Additional differences between these two types of turbines in terms of thermal characteristics can be shown with the help of Biot numbers summarized in Table 4. It is clearly seen that, as a result of the higher heat transfer coefficient, heat conduction inside the conventional rotor body offers much higher thermal resistance than the heat convection at the surface. Thermal resistance for the heat conduction of the nuclear rotor is less variable for the majority of start-up time as compared with the conventional rotor.

Table 4: Comparison of Biot numbers for nuclear and conventional turbines.

Turbine type	Biot number		
	0 rpm	50% load	100% load
Nuclear	302.5	292.3	290.3
Conventional	3.3	53.1	96.6

It is worth noting that Biot numbers obtained for the nuclear rotor are an order of magnitude larger than that considered as the threshold above which the variation of heat transfer coefficient has little influence on the variation of temperature distribution [31]. This fact justifies the use of a large and constant condensation heat transfer coefficient.

5 Summary

Small modular reactors are characterized by a wider range of possible applications than large nuclear reactors and the ability to flexible operation as per load demand. However, this greater flexibility results in more stringent design requirements for most components of the power plant equipped with this type of nuclear reactor.

This paper presented the numerical analysis of the thermal loads of a steam turbine rotor operating in a power plant with an SMR. The calculations performed included transient operation and a detailed analysis of cold start-up was conducted. The cold-start diagram was developed based on start-up diagrams of conventional units and accounting for the thermal characteristics of nuclear reactors.

A thermal cycle was proposed for a 300 MW SMR unit together with a steam turbine train consisting of the single flow HP module and two double flow LP modules. The HP module employs a drum-type rotor and 10 stages with reaction blading. The preliminary design rotor served as an object of detailed thermal investigations at transient operation.

Thermodynamic analysis has shown that steam throttling in the control valves results in steam superheating at the turbine inlet at the beginning of start-up which diminishes with time and saturated steam conditions are reached at a certain load. Even larger superheating exceeding 50°C occurs at the exhaust of the rotor balance piston and decreases during loading-up but is still around 1°C at full load. Steam superheating decreases with time along the steam path and at the HP turbine exhaust saturated steam conditions are present during the whole start-up (similar to the live steam condition).

These varying thermodynamic state of steam in the HP turbine is taken into account in thermal analyses and is shown to have a significant impact on the thermal load of the HP rotor under consideration. In particular, steam condensation on rotor surfaces plays a crucial role in determining its thermal behaviour.

The rotor temperature distributions obtained from turbine start-up simulations show that the highest metal temperatures, their rates of change and gradients occur at the rotor inlet sections, i.e. inlet channel, first blade grooves and the balance pistons. These are the most thermally loaded regions of the rotor where the largest heat fluxes from steam to the rotor surfaces are transferred.

It was also shown that the thermal loading of nuclear turbine rotors is lower and more stable than that of conventional rotors. Biot numbers calculated for nuclear rotors with high and constant condensation heat transfer coefficients are larger and more stable than those for conventional rotors.

Received 31 October 2023

References

[1] Qvist S., Gładysz P., Bartela Ł., Sowiżdżał A.: *Retrofit decarbonization of coal power plants – a case study for Poland*. Energies **14**(2021), 1, 120.

[2] International Atomic Energy Agency: *Energy, Electricity and Nuclear Power Estimates for the Period up to 2050, IAEA Reference Data Series No. 1*. IAEA-RDS-1/4, Vienna 2022.

[3] Kubowski J.: *Nuclear Power Plants*. WNT, Warszawa 2017 (in Polish).

[4] Chmielniak T.: *Power Generation Technologies*. PWN, Warszawa 2021 (in Polish).

[5] Dudek M., Jaszczur M., Kolenda Z.: *Thermodynamic analysis of modular high-temperature nuclear reactor coupled with the steam cycle for power generation*. Arch. Thermodyn. **40**(2019), 4, 49–66.

[6] Fic A., Składzień J., Gabriel M.: *Thermal analysis of heat and power plant with high temperature reactor and intermediate steam cycle*. Arch. Thermodyn. **36**(2015), 1, 3–18.

[7] Stanek W., Szargut J., Kolenda Z., Czarnowska L.: *Influence of nuclear power unit on decreasing emissions of greenhouse gases*. Arch. Thermodyn. **36**(2015), 1, 55–65.

[8] Rusanov A., Subotin V., Shvetsov V., Rusanov R., Palkov S., Palkov I., Chugay M.: *Application of innovative solutions to improve the efficiency of the LPC flow part of the 220 MW NPP steam turbine*. Arch. Thermodyn. **43**(2022), 1, 63–87.

[9] Bartela Ł., Gładysz P., Andreades C., Qvist S., Zdeb J.: *Techno-economic assessment of coal-fired power unit decarbonization retrofit with KP-FHR small modular reactors*. Energies **14**(2021), 9, 2557.

[10] Liou J.: *What are Small Modular Reactors (SMRs)?*. IAEA. https://www.iaea.org/newscenter/news/what-are-small-modular-reactors-smrs (accessed 14 Aug. 2023).

[11] Łukowicz H., Bartela Ł., Gładysz P., Qvist S.: *Repowering a coal power plant steam cycle using modular light-water reactor technology*. Energies **16**(2023), 7, 3083.

[12] Homa D., Kosman W., Bartela Ł.: *Cooperation of turbine island with 4^{th} generation nuclear reactor*. In: Proc. XXV Jubilee Cong. of Thermodynamicists, Gdańsk, 11-14 Sept. 2023, Book of papers (J. Cieśliński, D. Mikielewicz, J. Wajs, Eds.), 104–107. (in Polish).

[13] Irnational Atomic Energy Agency: *Advances in Small Modular Reactor Technology Developments. A Supplement to: IAEA Advanced Reactors Information System (ARIS)*. IAEA,Vienna 2022.

[14] Bartela Ł., Gładysz P., Ochmann J., Qvist S., Sancho L.M.: *Repowering a coal power unit with small modular reactors and thermal energy storage*. Energies **15**(2022), 16, 5830.

[15] Domański R.: *Modular nuclear reactors – state of knowledge and prospects*. In: Proc. XXV Jubilee Cong. of Thermodynamicists, Gdańsk, 11-14 Sept. 2023, Book of papers (J. Cieśliński, D. Mikielewicz, J. Wajs, Eds.), 72–75. (in Polish).

[16] Chmielniak T.: *Thermodynamic Cycles of Thermal Turbines*. Fluid-Flow Machinery Vol. 2. Ossolineum – Wydawn. PAN, Wrocław 1988 (in Polish).

[17] Perycz S.: *Steam and Gas Turbines*. Fluid-Flow Machinery Vol. 10. Ossolineum – Wydawn. PAN, Wrocław 1992 (in Polish).

[18] Ochmann J., Łukowicz H., Bartela Ł.: *Analysis of the influence of operating conditions of the steam turbine determined by location conditions on its operating characteristics*. In: Proc. XXV Jubilee Cong. of Thermodynamicists, Gdańsk, 11-14 Sept. 2023, Book of papers (J. Cieśliński, D. Mikielewicz, J. Wajs, Eds.), 239–242. (in Polish).

[19] International Atomic Energy Agency: *Status report 97 – Advanced Boiling Water Reactor (ABWR). IAEA Advanced Reactors Information System (ARIS)*, Jul 2011.

[20] *Status report 100 – Economic Simplified Boiling Water Reactor (ESBWR)*. IAEA Advanced Reactors Information System (ARIS). IAEA,Vienna 2021.

[21] GE Hitachi Nuclear Energy: *BWRX-300 General Description. Revision E*. 005N9751, 2023.

[22] Jun G., Kolovratnik M., Hoznedl M.: *Wet steam flow in 1100 MW turbine*. Arch. Thermodyn. **42**(2021), 3, 63–85.

[23] Laskowski R., Smyk A., Jurkowski R., Ance J., Wołowicz M., Uzunow N.: *Selected aspects of the choice of live steam pressure in PWR nuclear power plant*. Arch. Thermodyn. **43**(2022), 3, 85–109.

[24] Laskowski R., Smyk A., Ruciński A., Szymczyk J.: *Determining steam condensation pressure in a power plant condenser in off-design conditions*. Arch. Thermodyn. **42**(2021), 3, 45–62.

[25] Orlen: *Development program of BWRX-300 in Poland*, 2023. https://www.orlen.pl/pl/zrownowazony-rozwoj/projekty-transformacyjne/smr (accessed 10 Sept. 2023)

[26] Wacławiak K., Okrajni J.: *Transient heat transfer as a leading factor in fatigue of thick-walled elements at power plants*. Arch. Thermodyn. **40**(2019), 3, 43–55.

[27] Adamowicz A.: *Axisymmetric FE model to analysis of thermal stresses in a brake disc*. JTAM **53**(2015), 2, 357–370.

[28] Adamowicz A.: *Finite element anlysis of the 3D thermal stress state in a brake disc*. JTAM **54**(2016), 1, 205–218.

[29] Zienkiewicz O.C., Taylor R.L., Zhu J.Z.: *The Finite Element Method: It's Basis and Fundamentals*. Elsevier Butterworth-Heinemann, Burlington 2005.

[30] Hetnarski R.B., Eslami M.R.: *Thermal Stresses – Advanced Theory and Applications*. Springer, 2009.

[31] Chmielniak T., Kosman G.: *Thermal Loads of Steam Turbines*. WNT, Warszawa 1990 (in Polish).

[32] Banaszkiewicz M.: *Numerical investigation of crack initiation in the impulse steam turbine rotors subjected to thermo-mechanical fatigue*. Appl. Therm. Eng. **138**(2018), 761–773.

[33] Banaszkiewicz M.: *On-line determination of transient thermal stresses in critical steam turbine components using a two-step algorithm*. J. Therm. Stresses **40**(2017), 6, 690–703.

[34] Marinescu G., Ehrsam A., Sell M., Brunner P.: *Experimental investigation into thermal behaviour of steam turbine components. Part 3 – startup and the impact on LCF life*. In: Proc. ASME Turbo Expo 2013, San Antonio, June 3-7, 2013.

[35] Banaszkiewicz M., Badur J.: *Practical methods for online calculation of thermoelastic stresses in steam turbine components*. In: Selected Problems of Contemporary Thermomechanics (J. Winczek, Ed.), IntechOpen, 2018, 45–63.

[36] Taler J., Duda P.: *Solving Direct and Inverse Heat Conduction Problems*. Springer, Berlin Heidelberg 2006.

[37] Pilarczyk M., Weglowski B, Nord L.O.: *A comprehensive thermal and structural transient analysis of a boiler's steam outlet header by means of a dedicated algorithm and FEM simulation*. Energies **13**(2020), 1, 111.

[38] Shah M.M.: *A general correlation for heat transfer during film condensation inside pipes*. Int. J. Heat Mass Transf. **22**(1979), 547–556.

[39] Banaszkiewicz M.: *Steam turbines start-ups*. Trans. Inst. Fluid-Flow Mach. **126** (2014), 169–198.

[40] Rusin A., Banaszkiewicz M.: *Control and optimisation of 18K360 turbine start-up*. In: Proc. VI Sci.-Tech. Conf. Thermal Plants – Operation, Modernizations, Overhauls, Słok n/Bełchatow, 4-6 June, 2003 (in Polish).

[41] Banaszkiewicz M.: *Turbine thermal stress controller for retrofits of 370 MW units*. In: Proc. VIII Sci.-Tech. Conf. Thermal Plants – Operation, Modernizations, Overhauls, Słok n/Bełchatow, 21-23 May, 2007 (in Polish).

[42] Abaqus 6.13 user manual.